catalysts

MDPI

Article

High-Loaded Nickel Based Sol–Gel Catalysts for Methylcyclohexane Dehydrogenation

Yuliya K. Gulyaeva *, Maria V. Alekseeva (Bykova), Dmitry Yu. Ermakov, Olga A. Bulavchenko, Olesya O. Zaikina and Vadim A. Yakovlev

Boreskov Institute of Catalysis SB RAS, Pr. Akad. Lavrentieva, 5, 630090 Novosibirsk, Russia; bykova@catalysis.ru (M.V.A.); erm@catalysis.ru (D.Y.E.); isizy@catalysis.ru (O.A.B.); omironenko@catalysis.ru (O.O.Z.); yakovlev@catalysis.ru (V.A.Y.)

* Correspondence: gulyaeva@catalysis.ru

Received: 25 September 2020; Accepted: 12 October 2020; Published: 16 October 2020

Abstract: Application of liquid organic hydrogen carriers, such as "methylcyclohexane (MCH)–toluene" chemical couple, is one of the promising approaches for hydrogen storage and transportation. In the present study, copper-modified nickel catalysts with high metal loading of 75 wt% were synthesized via heterophase sol–gel technique, and investigated in the dehydrogenation of MCH. Two approaches towards the copper introduction were applied. The catalyst samples prepared via wetness impregnation of the nickel sol–gel catalyst are characterized by more effective Ni-Cu interaction compared to those where two metals were introduced simultaneously by the mixing of their solid precursors. As a result, the "impregnated" catalysts revealed higher selectivity towards toluene. The addition of copper up to 30 wt% of total metal content was shown to increase significantly toluene selectivity and yield without a noticeable decrease in MCH conversion. The catalyst with the active component including 80 wt% of Ni and 20 wt% of Cu demonstrated 96% and 89% toluene selectivity at 40% and 80% MCH conversion, respectively. Based on the obtained data, this non-noble catalytic system appears quite promising for the MCH dehydrogenation.

Keywords: dehydrogenation; methylcyclohexane; NiCu catalyst; LOHCs

1. Introduction

The growing interest in the use of alternative energy sources and energy carriers necessitates the development of approaches towards hydrogen storage and transportation [1,2]. One of the promising approaches is based on chemical binding of hydrogen (hydrogenation reaction) in the form of saturated hydrocarbons—liquid organic hydrogen carriers (LOHCs), e.g., cycloalkanes. Reversely, hydrogen can be drawn off by dehydrogenation of these species [2–6]. "Methylcyclohexane (MCH)—toluene (TOL)" cycle has been reported as a promising H_2 storage system that can be practically applicable on an industrial scale [7]. In this direction, catalytic membrane reactors of different geometries and membrane materials have been suggested to overcome thermodynamic limitations and increase MCH conversion [8–10]. Moreover, an integrated system that can provide energy for the MCH dehydrogenation maintaining a highly efficient cycle as the hydrogen-based power generation system has been proposed [11].

With regard to hydrogen supply and production, one of the most important issues is the choice of a system, which would effectively and selectively catalyze dehydrogenation reaction. Many studies have been focused on developing stable and active dehydrogenation catalysts primarily based on Pt or other precious metals supported on alumina [3,6,12–15]. Nonetheless, the high cost of noble metals prompted researchers to lower their use (particularly platinum) and/or to find alternatives. Therefore, numerous efforts have been made to substitute noble metals. In this case,

the cost-effective and widely available nickel-based catalysts proved to be highly promising [16,17]. However, the monometallic nickel-based catalysts are well-known to exhibit low selectivity and stability in dehydrogenation due to high hydrogenolysis reaction rates, which in turn results in decreasing yield of hydrogen [18,19]. The activity of nickel in hydrogenolysis transformations can be significantly reduced by the introduction of copper [20,21]. For example, when using Ni-Cu bimetallic catalysts in cyclohexane dehydrogenation, a significant increase in the selectivity of benzene formation (up to 99%) along with decreasing methanation efficiency was observed in comparison to the monometallic Ni-based system [18]. In contrast to cyclohexane, methyl-substituted cyclohexane is dehydrogenated at lower temperatures with the formation of toluene, which is considered to be much less carcinogenic compared to benzene [22]. This makes methylcyclohexane a more promising LOHC than cyclohexane [5]. On the other hand, due to the ease of breaking the C-C bond in the C_6H_{12}-CH_3 position, the contribution of the hydrogenolysis route becomes more significant for MCH [23]. So far, only a few studies on MCH dehydrogenation using nickel-based catalysts have been reported. Here, improved performance of Ni-based catalysts was also observed after the addition of a second metal. Al-ShaikhAli et al. showed that the introduction of the second metal (Ag, Sn, Zn, In) results in reduced conversion of methylcyclohexane, while selectivity to toluene increases in all cases [23,24]. The most selective catalyst in the considered series was $NiZn/Al_2O_3$, which demonstrated toluene selectivity of about 96–97% at MCH conversion of 32% in a continuous flow testing. This selectivity value was higher than that of the monometallic nickel sample (67%). Patil et al. investigated bimetallic NiCu/ACC (activated carbon cloth) catalysts and showed that a certain amount of copper (Ni/Cu = 8/2) suppresses the rate of hydrogenolysis, thereby increasing toluene selectivity and hydrogen yield [25]. For the NiCu/ACC catalyst in the spray pulse reactor, selectivity towards toluene was 75%, whereas MCH conversion did not exceed 25%. In general, all these catalytic systems with 10 wt% metal content demonstrated higher selectivity compared to monometallic nickel catalysts. However, these results were achieved at a moderate conversion of MCH (25–30%). Moreover, such nickel-based catalysts were noted to be less active compared to Pt [2,26]. Bearing all this in mind, the development of nickel-based catalysts with high nickel loading and modification by other metals might be an option for effective use in the dehydrogenation process. To make this approach relevant, it is especially important to provide high dispersion of the active metal particles. It certainly appears challenging in the case of a high metal loading and requires the implementation of a suitable catalyst preparation technique.

Such an approach—the so-called heterophase sol–gel synthesis—has been developed recently towards the preparation of nickel–copper catalysts [27–29]. It is based on the mixing of insoluble active component precursors and their activation, followed by a sol–gel formation. The catalysts obtained by this technique can have a high content of the active component (up to 75 wt%) with simultaneous maintaining its high dispersion, which is impossible to attain in the case of conventional impregnation methods. High-loaded $NiCu\text{-}SiO_2$ catalysts obtained by this technique revealed excellent performance in the liquid-phase hydrotreatment of bio-oil and its model compounds [29–31]. It is to be noted that an important advantage of the bimetallic Ni-Cu catalytic systems is their high reducibility under hydrotreatment process conditions and low activity towards undesirable methanation. Moreover, for dehydrogenation catalysts, in contrast to a well-known and widely used supporting material—alumina—using SiO_2 as an inert stabilizer for the active component is expected to provide a reduced tendency to coke formation. Since the heterophase sol–gel technique makes it possible to provide the high dispersion of active component along with the high metal loadings in the catalyst, using such an approach might open up the prospects to carry out the dehydrogenation process in a flow mode at high LHSV values. Moreover, it is expected to provide a high conversion of a selected LOHC at low catalyst loadings in the reactor. The uniqueness of this approach proposed towards the preparation of dehydrogenation catalysts became the key difference of the present study from all previous reports.

Thus, in the present work, a new type of nickel-based catalyst, prepared by the heterophase sol–gel technique, was studied in the dehydrogenation of methylcyclohexane. Moreover, the effect of copper

on the selectivity of thus prepared high-loaded (75 wt%) nickel catalysts was specifically addressed, with a special focus on the formation of toluene and side hydrogenolysis reactions. In particular, two approaches were used to synthesize the catalysts, and their main difference was associated with the method of copper introduction. One of the approaches included mixing the solid precursors of the active component—water-insoluble copper and nickel salts. The metal precursors subsequently reacted with a silicon-containing agent in the sol-preparation step. The second approach not applied previously was based on the introduction of copper by impregnating the as prepared nickel sol–gel catalyst.

2. Results and Discussion

2.1. Catalyst Characterization

Two series of catalysts denoted as SG- and pCu-series were prepared in this study following the method of copper introduction. For the SG-series, copper was introduced directly at the heterophase sol–gel stage, while for the pCu-series it was implemented by the impregnation of oxidized nickel sample. Additionally, a monometallic nickel catalyst SG_Ni-SiO_2 was prepared for comparison reasons. The catalysts for both the physicochemical characterization and catalytic tests were treated at the same temperature of 400 °C, based on the temperature-programmed reduction (TPR) of oxidized catalysts (vide infra). In the former case, the samples were reduced ex situ followed by passivating with ethanol. In the latter case, the reduction was performed in situ in the reactor prior to MCH dehydrogenation. Table 1 presents nickel and copper loadings in each catalyst series (for oxidized state), as well as Brunauer–Emmett–Teller specific surface area (A_{BET}) and CO pulsed chemisorption data onto the reduced catalysts. Despite the high content of the active component—Ni—all catalysts possess a high specific surface area, which slightly changes after the reductive treatment. Moreover, lower A_{BET} values for the pCu-series, if compared with the SG ones, at the same Ni/Cu ratio, are very likely due to an additional calcination step after the sequential deposition of copper. The data of CO pulsed chemisorption onto the reduced catalyst samples are expressed in μmols of CO per g of catalyst. Since CO can be adsorbed onto the metallic nickel species in various modes (linear, bridged, and carbonyl type) [32], the data obtained cannot allow a proper assessment of the active surface area. However, these data still open the prospects for a comparative analysis of the samples. In both series, with the copper content increase, a decrease in the amount of adsorbed CO is noted. It may be related to a higher surface concentration of copper, while the CO adsorption capacity of this metal is known to be lower than that of nickel [32,33].

High-resolution transmission electron microscopic (HRTEM) images of the reduced and passivated catalysts are presented in Figure 1 (for better quality images see Figure S1 in Supplementary Materials). The microphotographs revealed the presence of silicate-alike lamellar structures typical of sol–gel Ni-based catalytic systems [34]. The presence of uniformly distributed particles of 2–5 nm in size was shown, with the lattice parameters of these species corresponding to metallic nickel and nickel oxide. A small amount of single copper particles with a size of ~100 nm were found in the micrographs. At the same time, in most of the HRTEM images, no large particles were observed, while the EDX data for corresponding areas revealed the presence of nickel and copper (Figure S1 in Supplementary Materials). These data might be an indication of the high dispersion of copper in the samples. Moreover, the possibility of the formation of bimetallic solid solutions cannot be excluded. To provide evidence of the formation of such bimetallic solid solutions, the temperature-programmed reduction (TPR) and X-ray diffraction (XRD) investigations of SG and pCu series were performed. In general, it is to be noted that no significant differences in morphology between the two considered catalyst series were found by the HRTEM study.

Table 1. Catalyst composition in the oxidized state, Brunauer–Emmett–Teller specific surface area of the catalysts in oxidized ($A_{BET}{}^1$) and reduced form ($A_{BET}{}^2$), and CO chemisorption onto the reduced catalysts.

Sample	Metal Loading, wt%		$A_{BET}{}^1$, m^2/g	$A_{BET}{}^2$, m^2/g	μmol CO/g
	Ni	Cu			
SG_Ni-SiO_2	62.3	-	315	294	555
SG_Ni95Cu5-SiO_2	59.3	3.0	312	163	449
SG_Ni90Cu10-SiO_2	56.1	6.3	296	293	421
SG_Ni80Cu20-SiO_2	49.9	12.5	264	259	385
pCu_Ni95Cu5-SiO_2	59.9	3.3	301	234	384
pCu_Ni90Cu10-SiO_2	57.4	6.4	287	262	358
pCu_Ni80Cu20-SiO_2	52.2	13.0	225	235	266
pCu_Ni70Cu30-SiO_2	46.7	19.9	161	157	213

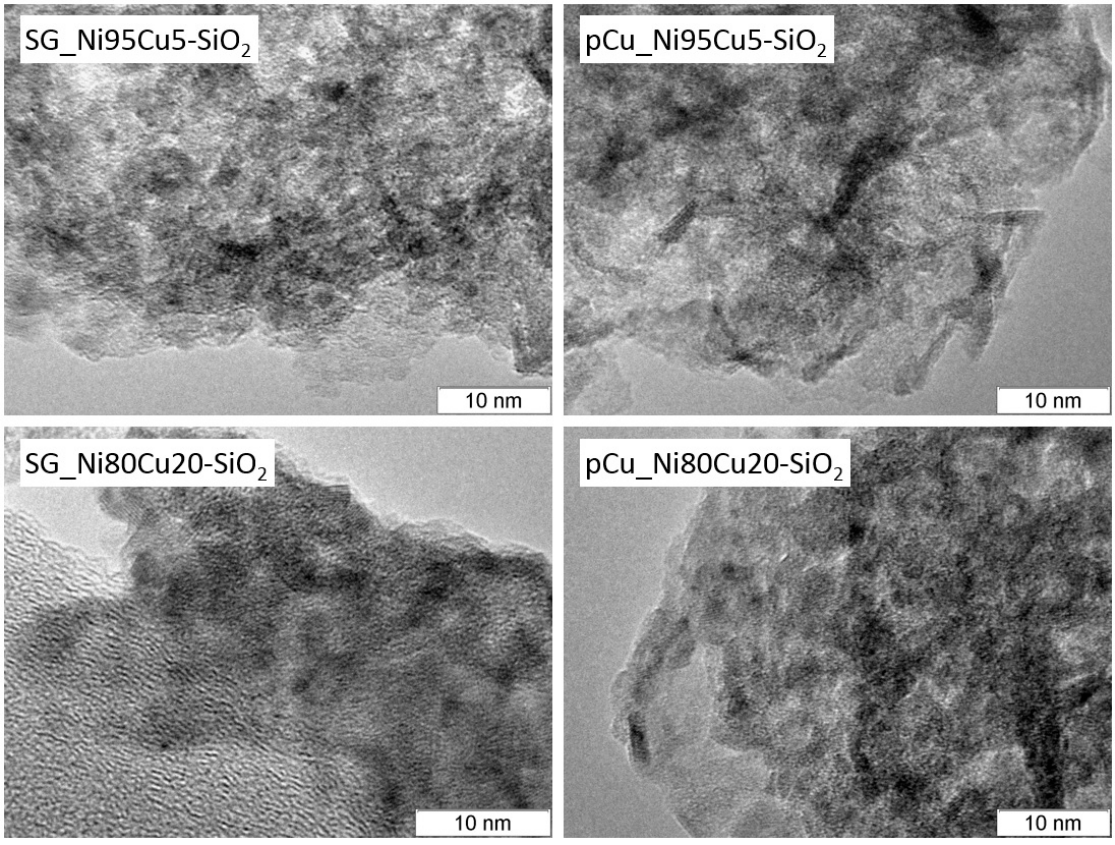

Figure 1. HRTEM images of SG_Ni95Cu5-SiO_2, pCu_Ni95Cu5-SiO_2, SG_Ni80Cu20-SiO_2, and pCu_Ni80Cu20-SiO_2 catalysts after reduction at 400 °C and passivation. Images of better quality are presented in Supplementary Materials.

The temperature-programmed reduction allows the indirect assessment of the effectiveness of interaction between the catalyst components, which is an important factor determining catalytic properties. Several hydrogen absorption maxima can be distinguished in the TPR curves of considered samples (Figure 2). For all catalysts, a low-temperature absorption peak is observed at 150–170 °C, associated with the reduction of Ni (III) species [35]. The formation of Ni (III) in turn is due to the chemisorption of oxygen onto a highly dispersed NiO. A wide absorption peak in the range of 350–700 °C points out at the effective interaction between nickel and silicon in these catalysts with the formation of hardly reducible silicate-alike structures [36–38]. All catalysts demonstrate this high-temperature wide absorption peak, as well as the peak at 300–320 °C assigned to the reduction

of NiO weakly bound to silicon [35,39]. In contrast to the monometallic catalyst, the TPR curves of copper-modified samples exhibit maxima at 220–230 °C and 240–280 °C. It is known that the reduction of nickel oxide in the presence of copper is shifted to lower temperatures [40,41]. For example, Naghash et al. showed that nickel oxide is reduced at temperatures up to 300 °C [41]. This induced reduction was clearly associated with the formation of solid oxide solutions [42]. Naghash et al. assumed that the introduction of copper leads to a decreasing strength of the Ni–O bond. This factor was suggested to determine the observed decrease in the reduction temperature. As for the reduction of oxidized copper species, it was shown to proceed at temperatures of 190–280 °C [40]. Thus, the peaks in the range of 200–300 °C in the recorded TPR curves were assigned to the reduction of copper oxide as well as the low-temperature reduction of nickel induced by copper.

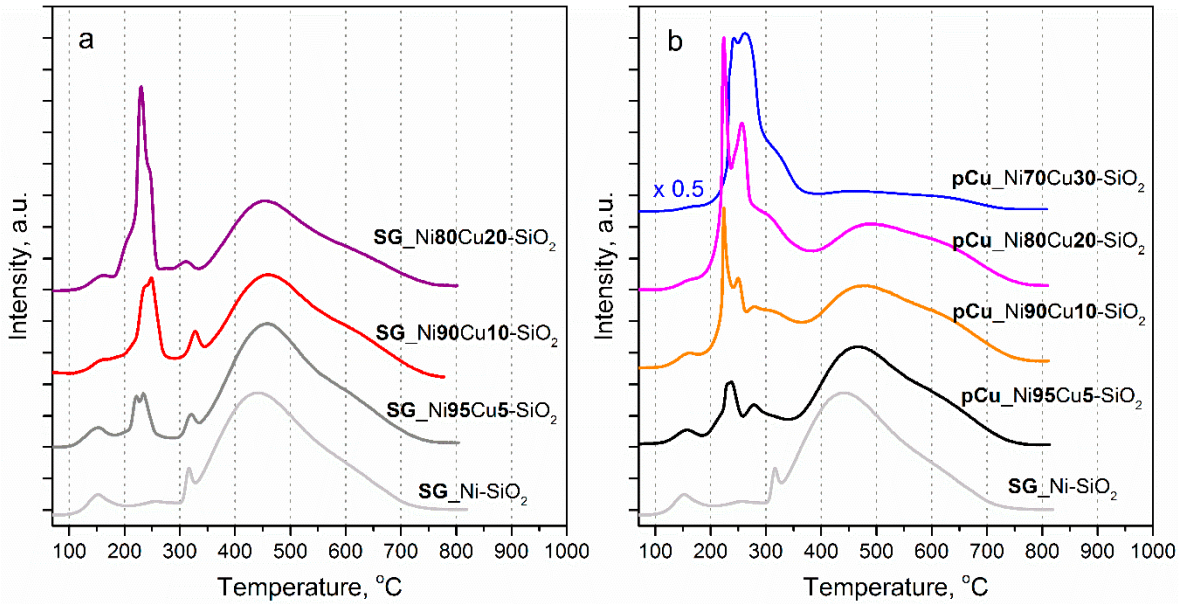

Figure 2. Temperature-programmed reduction (TPR) profiles of the SG (**a**) and pCu (**b**) series of catalysts with different Ni:Cu ratios. Conditions: m_{cat} = 50 mg, 10 vol.% H_2 in Ar, V_T = 6°/min.

The differences in the pCu-series reduction in the temperature range of 200–320 °C are of separate notice. The absorption peak ascribed to the low-temperature reduction of Ni (II) induced by copper is much more pronounced for the pCu-series compared to the SG-series. At the same time, the peak at 300–320 °C, attributed to the reduction of NiO weakly bound to silica becomes a shoulder and almost does not stand out. In addition, increasing copper content in the pCu-series results in increasing reduction ability in the region of 240–280 °C. Herewith, the relative intensity of the broad peak at 350–700 °C, assigned to the reduction of nickel effectively bonded to silica, simultaneously decreases. This observation clearly indicates a more efficient interaction of copper with nickel in pCu catalysts compared to SG samples.

The XRD patterns of oxidized catalysts (Figure 3) revealed wide NiO [JCPDS no. 471049] and sharp CuO [JCPDS no. 05-661] reflections. Moreover, no significant differences between the SG- and pCu-series for the shape of NiO reflections were observed. The coherent-scattering domain (CSD) size of nickel oxide does not change substantially when passing from one series to another (Table S1). This observation very likely indicates that the preparation method does not cause any significant effects in the considered range of Ni:Cu atomic ratios, even in the case of an additional calcination stage applied to the pCu-series. In the case of the pCu_Ni70Cu30-SiO_2 sample, the shape of NiO reflections was not typical most likely due to the bimodal distribution of NiO particle sizes.

For the pCu-series, the relative intensity of CuO reflections was lower compared to SG catalysts at close Ni:Cu ratios (Figure 2). This is especially noticeable for the SG_Ni95Cu5-SiO_2 catalyst: CuO reflections in the XRD pattern of this sample are much more pronounced than those observed for

the pCu-series at the same copper content. Moreover, the CSD sizes of CuO phase for the pCu catalysts were larger than those for the corresponding SG catalysts. For the pCu_Ni95Cu5-SiO_2 catalyst, the CSD size of CuO could not be estimated due to a relatively low reflection intensity.

A similar trend was observed for the catalysts reduced at 400 °C followed by passivation (Figure 3). It is obvious that the intensity of Cu reflections in relation to Ni ones in the pCu_Ni95Cu5-SiO_2 catalyst is significantly lower than in the case of SG_Ni95Cu5-SiO_2. For the higher copper content, this trend continues. At the same copper content in the catalyst pairs, the large well-crystallized CuO particles are present in pCu samples in lesser amounts if compared to the SG-series. However, it is these large particles, which are mainly contributing to high CSD values. Most likely, in the case of pCu catalysts, finely dispersed and hence X-ray amorphous particles of CuO and Cu are preferentially formed. Moreover, the presence of unreduced NiO was noted in the diffraction patterns of the reduced samples, in addition to metallic Ni and Cu phases. This is in good agreement with the TPR data, which revealed that the reduction of oxidized metal species can proceed up to 700 °C. The absence of peaks corresponding to copper oxide confirms that CuO is completely reduced under the selected conditions.

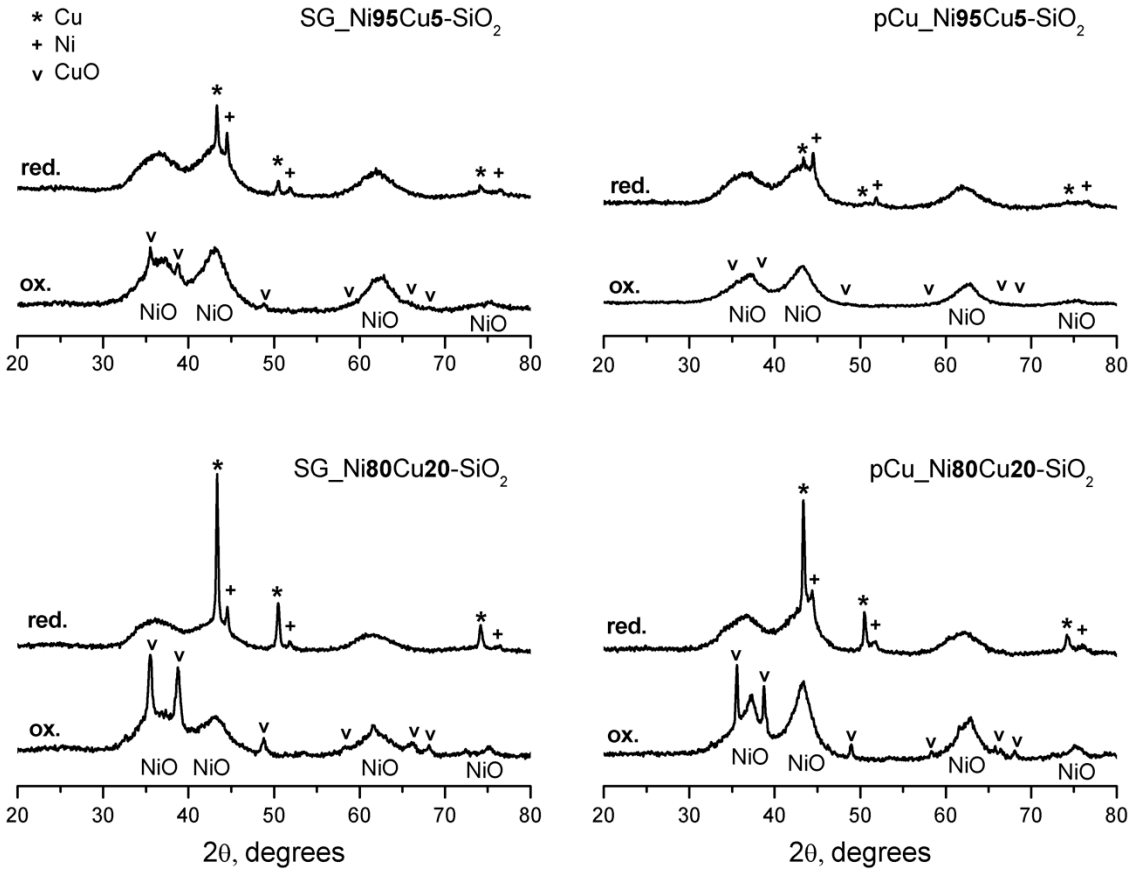

Figure 3. X-ray diffraction patterns of the catalysts SG_Ni95Cu5-SiO_2, SG_Ni80Cu20-SiO_2, pCu_Ni95Cu5-SiO_2, and pCu_Ni80Cu20-SiO_2, before (ox.) and after reduction (red.).

Based on 111 reflections, the lattice parameters of Ni were estimated as 3.526 Å and 3.540 Å for the SG_Ni80Cu20-SiO_2 and pCu_Ni80Cu20-SiO_2 samples, respectively. The obtained values appeared to be higher than the published data for the lattice of metallic nickel a = 3.523 Å [JCPDS no. 040850], which points to the formation of solid nickel–copper solutions [20,43]. Moreover, these data provide additional evidence of the formation of solid solutions previously noted for the nickel–copper catalysts obtained by the heterophase sol–gel technique [29,30,39]. It is to be additionally emphasized that in the case of the pCu_Ni80Cu20-SiO_2 catalyst, the lattice parameter of Ni is significantly increased with

respect to the literature data. It points out the formation of a solid solution with a high copper content ($Ni_{0.8}Cu_{0.2}$ according to the Vegard's law and the data of Sinfelt et al. [20]).

Thus, the data obtained indicate an effective interaction between nickel and copper in the catalysts concerned, which can significantly affect their catalytic properties. In addition, the data of XRD and TPR studies point out a more even distribution of copper in the pCu catalysts, in contrast to the SG approach. Apparently, in the former type of catalyst, more efficient interaction between the two metals is provided as a result of the formation of a solid nickel–copper solution.

2.2. Catalyst Activity in MCH Dehydrogenation

Figure 4 shows the comparative performance of the catalysts in MCH dehydrogenation versus reaction temperature. It is evident that with increasing reaction temperature, MCH conversion increases as well in the presence of the monometallic nickel-based catalyst. At that, an extremely low selectivity to toluene formation is observed, in agreement with previously reported results for the dehydrogenation of cycloalkanes over a monometallic nickel catalyst [18,24]. The main by-products are methane and benzene, which is indicative of the competing dealkylation of MCH with increasing temperature. When passing to the copper-modified catalysts, a marked increase in toluene selectivity is evidenced, compared to the monometallic system. The relative increase in selectivity and yield of toluene for copper-modified catalysts becomes even more pronounced at temperatures above 275 °C, intrinsically related to higher conversion.

As is evident from Figure 4a, a slight decrease in MCH conversion occurs with the increase in copper content. For the pCu_Ni95Cu5-SiO_2, pCu_Ni90Cu10-SiO_2, and monometallic SG_Ni-SiO_2 catalysts, the yield of toluene increases for the temperatures up to 300 °C, with a sharp decrease thereafter. At the same time, for the samples with higher copper content, the toluene yield continues to increase at 325 °C. Moreover, an increase in the yield of dealkylation products (benzene, methane) was noted for all catalysts at high conversion. However, the yield of by-products in the case of pCu_Ni80Cu20-SiO_2 was 3–5 times lower than for the samples with lower copper contents. In general, it should be emphasized that the introduction of copper into the nickel-based catalyst helps to reduce the contribution of the MCH dealkylation reaction at elevated temperatures. Additionally, while considering the dependence of toluene yield on copper content (See Figure S2 in Supplementary Materials) at specific reaction temperatures, the yield of toluene is observed to constantly increase at 325 and 350 °C (in accordance with increasing MCH conversion). Herewith, the maximum yield of toluene was achieved over the pCu_Ni80Cu20-SiO_2 and pCu_Ni70Cu30-SiO_2 catalysts at 325 °C.

Figure 4b shows the results obtained over the SG-series. Here, one of the most interesting samples in the pCu-series—pCu_Ni80Cu20-SiO_2 sample—is given as well for the ease of comparison between the two series. It can be observed that a slightly higher MCH conversion is observed over SG_Ni80Cu20-SiO_2 compared to pCu_Ni80Cu20-SiO_2 at temperatures up to 300 °C (Figure 3). Most likely, this could be due to the larger specific surface area of the active component in the former case (Table 1). Nonetheless, the pCu_Ni80Cu20-SiO_2 sample seems to be more promising in comparison with the corresponding SG catalyst, based on the MCH conversion, as well as toluene selectivity and yield. When the temperature is higher than 300 °C, the MCH conversion over SG catalysts reaches 80–90%, giving a noticeable decrease in the toluene yield in accordance with a significantly decreasing selectivity. In contrast, it is likely that the effective interaction of copper with nickel in the pCu catalysts leading to the formation of nickel–copper solid solution provides higher selectivity of these catalysts towards toluene.

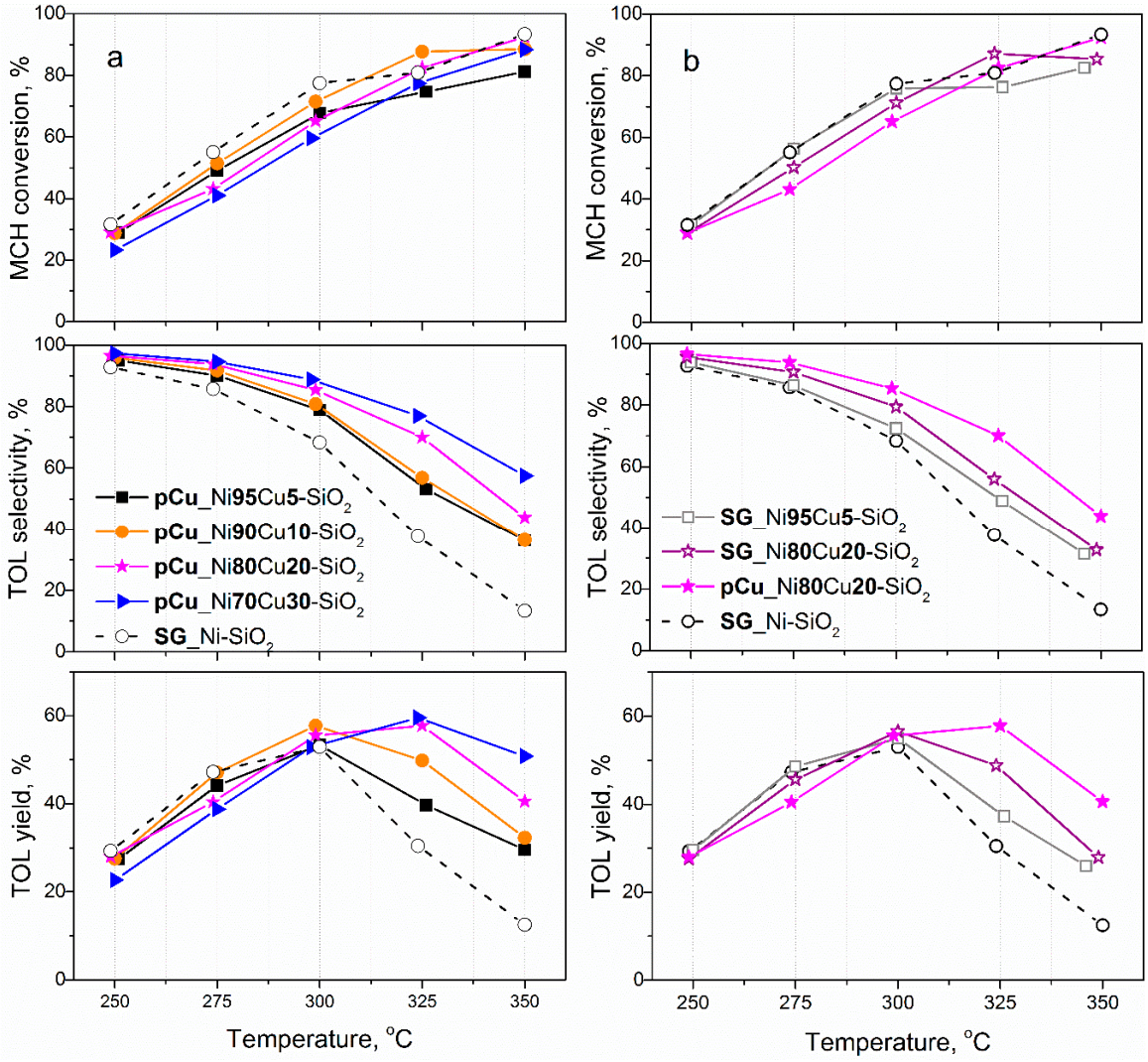

Figure 4. Comparative catalytic performance of pCu (**a**) and SG (**b**) catalyst series in methylcyclohexane (MCH) dehydrogenation. TOL means toluene. Reaction conditions: T = 250–350 °C, P = 0.1 MPa, m_{cat} = 0.50 g, H_2/Ar molar ratio equal to 1, gas feed rate of 400 mL/min, liquid feed rate of 12 mL/h.

Thus, for the pCu_Ni80Cu20-SiO_2 catalyst, a significant decrease in the concentration of hydrogenolysis products was demonstrated at considerably high MCH conversions (X above 70%), compared to the catalysts with lower copper loadings (pCu_Ni90Cu10-SiO_2 and pCu_Ni95Cu5-SiO_2). For this catalyst, to verify whether the high selectivity to toluene can be achieved at moderate temperatures ensuring high conversion levels, the experiments at higher contact time (WHSV was decreased from 18.5 to 4.6 h^{-1}) were performed at 250 and 275 °C, respectively. Moreover, in these runs, the catalysts were tested within 20 h on stream at a constant reaction temperature (Figure 5). The data obtained reveal that the catalyst retains a sufficiently high activity for the 20 h testing. An important observation is made about the catalyst selectivity towards toluene reaching 96% at MCH conversion of 40% at 250 °C. Moreover, the toluene selectivity is maintained sufficiently high (89%) even at higher MCH conversions of 75–80% at 275 °C. It was also found that such high activity and selectivity results have not been reported for MCH dehydrogenation so far. For example, Patil et al. [25] managed to achieve a toluene selectivity of about 75% at MCH conversion of 25% using NiCu/ACC catalyst. The process was carried out in a spray pulse reactor in the absence of a carrier gas. Al-ShaikhAli et al. [23,24] demonstrated that the most promising zinc-modified catalyst NiZn/Al_2O_3 showed a quite high selectivity of 96–97%, however, the MCH conversion did not exceed 32%. These data

were obtained in a flow reactor, while the process was carried out in the presence of hydrogen and argon. However, it is to be taken into account that, in view of the different conditions used, it is impossible to make a proper comparison of quantitative data between those studies and the present work. Nevertheless, the results obtained allow us to conclude that pCu_Ni80Cu20-SiO_2 catalytic system is not inferior to the most promising Ni-based catalysts of MCH dehydrogenation obtained so far.

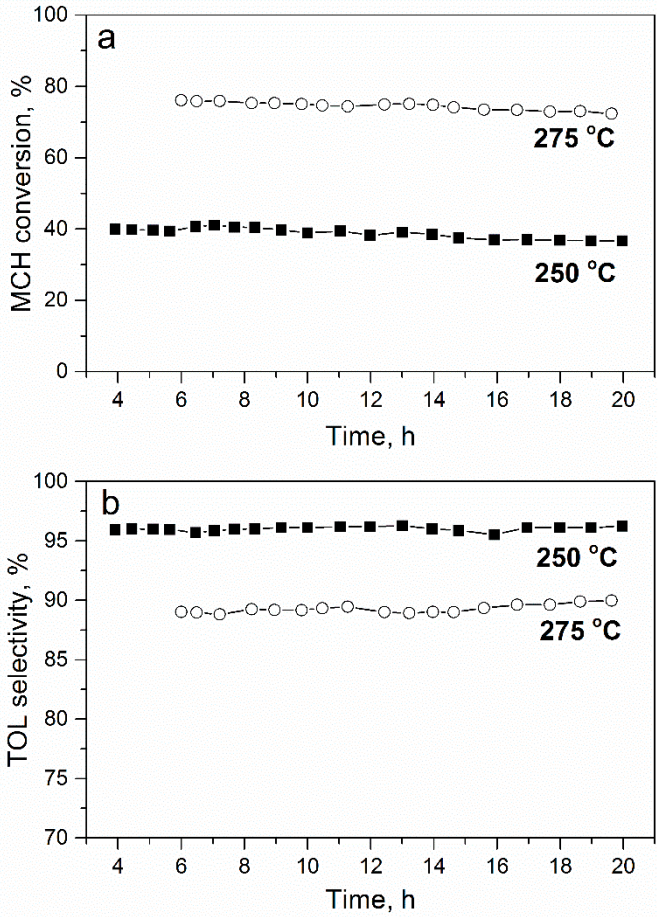

Figure 5. Methylcyclohexane (MCH) conversion (**a**) and toluene (TOL) selectivity (**b**) as a function of time over pCu_Ni80Cu20-SiO_2 catalyst. Reaction conditions: T = 250 and 275 °C, P = 0.1 MPa, m_{cat} = 1.00 g, H_2/Ar molar ratio equal to 1, gas feed rate of 400 mL/min, liquid feed rate of 6 mL/h.

3. Materials and Methods

3.1. Catalyst Preparation

Bimetallic nickel–copper catalysts were prepared using the heterophase sol–gel technique similar to that reported previously [27,44], with SiO_2 acting as a stabilizer of the active component. Two approaches were used to synthesize the catalysts. One of them was based on the joint introduction of heterogeneous metal precursors at the sol–gel stage. For the catalysts with different atomic ratios of Ni/Cu, solid active component precursors $NiCO_3 \cdot mNi(OH)_2 \cdot nH_2O$ and $CuCO_3 \cdot mCu(OH)_2$ were mixed with bi-distilled water and aqueous ammonia. In the case of a monometallic nickel catalyst, a copper-containing agent was not added to the reaction mixture. Then, ethyl silicate was added to the suspension under constant stirring. The mixture was aged for 30 min, then dried at 100 °C for 12 h and calcined at 400 °C for 4 h in air (8 °C/min). The second approach was based on the impregnation of a monometallic nickel catalyst with a solution of copper nitrate followed by the same drying and calcination procedure. This "impregnation" approach was applied to high-loading nickel–copper catalysts for the first time.

For the physicochemical investigation, the catalysts were reduced by H_2 (500 mL/min) in a quartz tube reactor at 400 °C for 1 h. Hereafter, the reactor was cooled down to room temperature, purged with argon, and the catalyst was passivated with ethanol.

The catalysts obtained according to the first method were designated as SG_NiXCuY-SiO_2, while those obtained via the second approach—pCu_NiXCuY-SiO_2. In this notation, X and Y correspond to a nominal percentage of nickel and copper relative to the total amount of metals.

3.2. Catalyst Characterization

3.2.1. Nitrogen Physisorption

Texture characteristics of catalysts were measured at the liquid nitrogen temperature using an ASAP-2400 automated volumetric adsorption analyzer (Micromeritics Instrument Corp., Norcross, GA, USA). Before the analysis, the samples were pretreated at 150 °C and pressure 0.13 Pa for 4 h. The analysis time was varied depending on the particular sample. The resulting adsorption isotherms were used to calculate the Brunauer–Emmett–Teller specific surface area (A_{BET}).

3.2.2. CO Pulse Chemisorption Measurements

CO pulse chemisorption measurements were carried out using a Chemosorb analyzer (Modern Laboratory Equipment, Novosibirsk, Russia). An amount of 50 mg of each catalyst was placed inside a U-shape quartz reactor and treated in an H_2 flow (100 mL/min) upon heating up to 400 °C. The reactor was kept at the final temperature for 20 min and then purged by inert gas (Ar) followed by cooling down to room temperature. After that, pulses of CO were fed to the reactor (100 μL) until the amount of CO in the outlet stopped changing according to the thermal conductivity detector. Thereafter the amount of chemisorbed CO was estimated.

3.2.3. Temperature-Programmed Reduction

Catalyst sample in the oxidized state (0.1 g) was placed in a U-tube quartz reactor and treated in a reducing atmosphere (10 vol.% of H_2 balanced in Ar at a flow rate of 20 mL/min) with a constant heating rate of 6°/min up to 800 °C. The hydrogen concentration in the outlet stream during the reduction was measured with a thermal conductivity detector.

3.2.4. High-Resolution Transmission Electron Microscopy

The microstructure of catalysts was examined by high-resolution transmission electron microscopy (HRTEM) on a JEM-2010 electron microscope (JEOL, Tokyo, Japan) at an accelerating voltage of 200 kV and point-to-point resolution of 0.14 nm. The microscope was equipped with an XFlash energy-dispersive X-ray (EDX) spectrometer (Bruker, Ettlingen, Germany) with energy resolution 200 eV. Before electron-microscopic examination, the particles were immersed in ethanol and prepared on a holey carbon film mounted on an aluminium grid. The particles were prepared using a UZD-1UCh2 ultrasonic processor, which allowed us to achieve a uniform distribution of the particles over the film surface.

3.2.5. X-ray Diffraction (XRD)

The phase composition of samples was studied on a D8 Advance X-ray diffractometer (Bruker, Ettlingen, Germany) using a monochromatic Cu$K\alpha$ radiation λ = 1.5418 Å with a step 2θ = 0.05° and accumulation time 3 s at each point. The diffractometer was equipped with a linear LynxEye (1D) detector. The mean size of the coherent-scattering domain (CSD) was calculated using the Selyakov-Scherrer equation, based on the half-width of the diffraction lines. The lattice parameters and the phase ratios were defined by the Rietveld method [45].

3.2.6. X-ray Fluorescence Analysis (XRF)

The elemental composition of oxide samples was determined using X-ray fluorescence spectrometer ARL Advant'X 2247 (Thermo Fisher Scientific, Waltham, MA, USA) equipped with Rh anode as an X-ray source. The mass percentage of elements was estimated using QuantAS software. All samples were analyzed by XRF in triplicate and the average values were reported.

3.3. Testing in MCH Dehydrogenation

Catalyst testing was carried out in a fixed bed flow reactor in a temperature range of 250–350 °C under atmospheric pressure. The reactor was loaded by 0.5 g of catalyst (fraction 0.25–0.5 mm) diluted with quartz of the same fraction to a volume of 3 mL. The catalyst was reduced in situ before the experiment at 400 °C for 1 h (H_2 flow of 500 mL/min), after which it was cooled down to 150 °C in a hydrogen stream. Methylcyclohexane, MCH, dehydrogenation was performed at a molar ratio of H_2/Ar = 1/1 and a total gas feed rate of 400 mL/min. MCH was supplied using a liquid pump at a rate of 12 mL/h. Liquid products and unreacted MCH were collected in the condensation system and analyzed with an Agilent Technologies 7820A chromatograph equipped with a flame ionization detector and a capillary column (Polyethylene Glycol, 30 m length, 0.25 mm inner diameter, 0.25 mm film thickness). The gas-phase was analyzed on-line using a Chromos-GC chromatograph equipped with a silochrome column (3 m × 2 mm i.d.) and flame ionization detector.

At higher contact time, continuous MCH dehydrogenation experiments (up to 20 h) were carried out using pCu_Ni80Cu20-SiO_2 at a preset reaction temperature (250 or 275 °C). A preliminary reduction of the catalyst (1 g) was performed under the same conditions as described above. The total volume of the catalyst together with quartz inert material was 6 mL, the gas flow rate was maintained 400 mL/min at H_2/Ar molar ratio of 1/1; MCH feeding rate of 6 mL/h.

Methylcyclohexane conversion (X_{MCH}), toluene selectivity (S_{TOL}), and toluene yield (W_{TOL}) were calculated according to the expressions:

$$X_{MCH}(\%) = \frac{C^0_{MCH} - C_{MCH}}{C^0_{MCH}} \times 100\%,$$

$$S_{TOL}(\%) = \frac{C_{TOL}}{C^0_{MCH} - C_{MCH}} \times 100\%,$$

$$W_{TOL}(\%) = \frac{C_{TOL}}{C^0_{MCH}} \times 100\%,$$

where C^0_{MCH} and C_{MCH} are the respective molar concentrations of MCH at the inlet and outlet of the reactor (in moles), C_{TOL} being the molar concentration of toluene at the outlet of the reactor.

4. Conclusions

In this study, the proposed high-loaded nickel–copper catalysts proved to be promising for MCH dehydrogenation. Herewith, despite high metal content, the heterophase sol–gel preparation approach allows one to obtain the nickel-based catalyst with a quite high specific surface area, which ensures the high activity of the catalysts in MCH dehydrogenation. The introduction of copper in the amount of up to 30% of the total metal content only slightly reduces the conversion of MCH. However, it significantly inhibits the efficiency of hydrogenolysis and increases the selectivity to the formation of dehydrogenation products. Additionally, the sequential introduction of copper into the nickel-based catalyst by impregnation (pCu) makes it possible to achieve a more even distribution of the second metal than in the case of Ni and Cu combined introduction from the solid precursors (SG). This, in turn, leads to a more efficient interaction between two metals due to the formation of a solid nickel–copper solution and provides high selectivity of pCu bimetallic catalysts in MCH

dehydrogenation. The catalyst with a Ni/Cu ratio of 80/20 revealed 96% and 89% selectivity towards toluene formation at high MCH conversions of 40% and 75–80%, respectively. Interestingly, such high selectivity values at high MCH conversions were not achieved over nickel-based catalysts previously. Moreover, the selectivity values for MCH dehydrogenation were demonstrated to be not changing within 20 h. The results obtained point out the prospectiveness of the heterophase sol–gel approach (combined with the second metal deposition by impregnation) to the synthesis of dehydrogenation catalysts. These data also open the prospects for further modification of the synthesis procedure, including the studies using other second metals and their introduction method, to ensure more uniform distribution and effective interaction with Ni. This is expected to allow the development of an active and selective non-noble metal catalyst for MCH dehydrogenation.

Supplementary Materials: The following are available online at http://www.mdpi.com/2073-4344/10/10/1198/s1, Figure S1: HRTEM images and corresponding EDX data (nickel and copper atomic percentages) for the catalysts after reduction at 400 °C and passivation, Figure S2: Dependence of toluene yield on copper fraction (wt%) in the pCu catalysts and SG_Ni-SiO_2 at different temperatures in the methylcyclohexane dehydrogenation. Copper fraction is a percentage of copper relative to the total amount of both metals (nickel and copper), Table S1: Phase composition and average size of coherent scattering region (CSD size, Å) for the catalysts in oxidized state.

Author Contributions: Conceptualization, V.A.Y. and Y.K.G.; formal analysis, Y.K.G. and M.V.A.; investigation, Y.K.G., M.V.A., D.Y.E., O.O.Z. and O.A.B.; visualization, Y.K.G. and O.A.B.; writing—original draft preparation, Y.K.G.; writing—review and editing, M.V.A. and V.A.Y. All authors have read and agreed to the published version of the manuscript.

Funding: This work was conducted within the framework of the budget project for Boreskov Institute of Catalysis.

Acknowledgments: The authors express gratitude to Evgeny Yu. Gerasimov for carrying out TEM analysis.

Conflicts of Interest: The authors declare no conflict of interest.

References

1. Dalebrook, A.F.; Gan, W.; Grasemann, M.; Moret, S.; Laurenczy, G. Hydrogen storage: Beyond conventional methods. *Chem. Commun.* **2013**, *49*, 8735–8751. [CrossRef] [PubMed]
2. Preuster, P.; Papp, C.; Wasserscheid, P. Liquid Organic Hydrogen Carriers (LOHCs): Toward a Hydrogen-free Hydrogen Economy. *Acc. Chem. Res.* **2017**, *50*, 74–85. [CrossRef] [PubMed]
3. Biniwale, R.B.; Rayalu, S.; Devotta, S.; Ichikawa, M. Chemical hydrides: A solution to high capacity hydrogen storage and supply. *Int. J. Hydrogen Energy* **2008**, *33*, 360–365. [CrossRef]
4. Gianotti, E.; Taillades-Jacquin, M.; Rozière, J.; Jones, D.J. High-Purity Hydrogen Generation via Dehydrogenation of Organic Carriers: A Review on the Catalytic Process. *ACS Catal.* **2018**, *8*, 4660–4680. [CrossRef]
5. Aakko-Saksa, P.T.; Cook, C.; Kiviaho, J.; Repo, T. Liquid organic hydrogen carriers for transportation and storing of renewable energy—Review and discussion. *J. Power Sources* **2018**, *396*, 803–823. [CrossRef]
6. Alhumaidan, F.; Tsakiris, D.; Cresswell, D.; Garforth, A. Hydrogen storage in liquid organic hydride: Selectivity of MCH dehydrogenation over monometallic and bimetallic Pt catalysts. *Int. J. Hydrogen Energy* **2013**, *38*, 14010–14026. [CrossRef]
7. Okada, Y.; Shimura, M. *Development of Large-Scale H_2 Storage and Transportation Technology with Liquid Organic Hydrogen Carrier (LOHC)*; Joint GCC-JAPAN Environment Symposium: Doha, Qatar, February 2013.
8. Itoh, N.; Watanabe, S.; Kawasoe, K.; Sato, T.; Tsuji, T. A membrane reactor for hydrogen storage and transport system using cyclohexane–methylcyclohexane mixtures. *Desalination* **2008**, *234*, 261–269. [CrossRef]
9. Wunsch, A.; Mohr, M.; Pfeifer, P. Intensified LOHC-Dehydrogenation Using Multi-Stage Microstructures and Pd-Based Membranes. *Membranes* **2018**, *8*, 112. [CrossRef]
10. Cholewa, M.; Zehner, B.; Kreuder, H.; Pfeifer, P. Optimization of membrane area to catalyst mass in a microstructured membrane reactor for dehydrogenation of methylcyclohexane. *Chem. Eng. Process. Process Intensif.* **2018**, *125*, 325–333. [CrossRef]
11. Juangsa, F.B.; Prananto, L.A.; Mufrodi, Z.; Budiman, A.; Oda, T.; Aziz, M. Highly energy-efficient combination of dehydrogenation of methylcyclohexane and hydrogen-based power generation. *Appl. Energy* **2018**, *226*, 31–38. [CrossRef]

12. Jothimurugesan, K.; Bhatia, S.; Srivastava, R.D. Kinetics of dehydrogenation of methylcyclohexane over a platinum-rhenium-alumina catalyst in the presence of added hydrogen. *Ind. Eng. Chem. Fundam.* **1985**, *24*, 433–438. [CrossRef]
13. Niermann, M.; Beckendorff, A.; Kaltschmitt, M.; Bonhoff, K. Liquid Organic Hydrogen Carrier (LOHC)—Assessment based on chemical and economic properties. *Int. J. Hydrogen Energy* **2019**, *44*, 6631–6654. [CrossRef]
14. Coughlin, R.W.; Kawakami, K.; Hasan, A. Activity, yield patterns, and coking behavior of Pt and PtRe catalysts during dehydrogenation of methylcyclohexane: I. In the absence of sulfur. *J. Catal.* **1984**, *88*, 150–162. [CrossRef]
15. Alhumaidan, F.; Cresswell, D.; Garforth, A. Hydrogen Storage in Liquid Organic Hydride: Producing Hydrogen Catalytically from Methylcyclohexane. *Energy Fuels* **2011**, *25*, 4217–4234. [CrossRef]
16. Biniwale, R.B.; Kariya, N.; Ichikawa, M. Dehydrogenation of Cyclohexane Over Ni Based Catalysts Supported on Activated Carbon using Spray-pulsed Reactor and Enhancement in Activity by Addition of a Small Amount of Pt. *Catal. Lett.* **2005**, *105*, 83–87. [CrossRef]
17. Hodoshima, S.; Nagata, H.; Saito, Y. Efficient hydrogen supply from tetralin with superheated liquid-film-type catalysis for operating fuel cells. *Appl. Catal. A* **2005**, *292*, 90–96. [CrossRef]
18. Xia, Z.; Lu, H.; Liu, H.; Zhang, Z.; Chen, Y. Cyclohexane dehydrogenation over Ni-Cu/SiO_2 catalyst: Effect of copper addition. *Catal. Commun.* **2017**, *90*, 39–42. [CrossRef]
19. Desai, P.H.; Richardson, J.T. Crystallite size effects in nickel catalysts: Cyclohexane dehydrogenation and hydrogenolysis. *J. Catal.* **1986**, *98*, 392–400. [CrossRef]
20. Sinfelt, J.H.; Carter, J.L.; Yates, D.J.C. Catalytic hydrogenolysis and dehydrogenation over copper-nickel alloys. *J. Catal.* **1972**, *24*, 283–296. [CrossRef]
21. Xia, Z.; Liu, H.; Lu, H.; Zhang, Z.; Chen, Y. Study on catalytic properties and carbon deposition of Ni-Cu/SBA-15 for cyclohexane dehydrogenation. *Appl. Surf. Sci.* **2017**, *422*, 905–912. [CrossRef]
22. Preuster, P.; Alekseev, A.; Wasserscheid, P. Hydrogen Storage Technologies for Future Energy Systems. *Annu. Rev. Chem. Biomol. Eng.* **2017**, *8*, 445–471. [CrossRef] [PubMed]
23. Al-ShaikhAli, A.H.; Jedidi, A.; Anjum, D.H.; Cavallo, L.; Takanabe, K. Kinetics on NiZn Bimetallic Catalysts for Hydrogen Evolution via Selective Dehydrogenation of Methylcyclohexane to Toluene. *ACS Catal.* **2017**, *7*, 1592–1600. [CrossRef]
24. Al-ShaikhAli, A.H.; Jedidi, A.; Cavallo, L.; Takanabe, K. Non-precious bimetallic catalysts for selective dehydrogenation of an organic chemical hydride system. *Chem. Commun.* **2015**, *51*, 12931–12934. [CrossRef] [PubMed]
25. Patil, S.P.; Pande, J.V.; Biniwale, R.B. Non-noble Ni–Cu/ACC bimetallic catalyst for dehydrogenation of liquid organic hydrides for hydrogen storage. *Int. J. Hydrogen Energy* **2013**, *38*, 15233–15241. [CrossRef]
26. Lang, C.; Jia, Y.; Yao, X. Recent advances in liquid-phase chemical hydrogen storage. *Energy Storage Mater.* **2020**, *26*, 290–312. [CrossRef]
27. Ermakov, D.Y.; Bykova, M.V.; Selisheva, S.A.; Khromova, S.A.; Yakovlev, V.A. Method of Preparing hydrotreatment Catalyst. Patent RU2496580C1, 8 October 2012.
28. Yakovlev, V.A.; Khromova, S.A.; Sherstyuk, O.V.; Dundich, V.O.; Ermakov, D.Y.; Novopashina, V.M.; Lebedev, M.Y.; Bulavchenko, O.; Parmon, V.N. Development of new catalytic systems for upgraded bio-fuels production from bio-crude-oil and biodiesel. *Catal. Today* **2009**, *144*, 362–366. [CrossRef]
29. Ardiyanti, A.R.; Bykova, M.V.; Khromova, S.A.; Yin, W.; Venderbosch, R.H.; Yakovlev, V.A.; Heeres, H.J. Ni-Based Catalysts for the Hydrotreatment of Fast Pyrolysis Oil. *Energy Fuels* **2016**, *30*, 1544–1554. [CrossRef]
30. Bykova, M.V.; Ermakov, D.Y.; Kaichev, V.V.; Bulavchenko, O.A.; Saraev, A.A.; Lebedev, M.Y.; Yakovlev, V.A. Ni-based sol–gel catalysts as promising systems for crude bio-oil upgrading: Guaiacol hydrodeoxygenation study. *Appl. Catal. B* **2012**, *113–114*, 296–307. [CrossRef]
31. Yin, W.; Kloekhorst, A.; Venderbosch, R.H.; Bykova, M.V.; Khromova, S.A.; Yakovlev, V.A.; Heeres, H.J. Catalytic hydrotreatment of fast pyrolysis liquids in batch and continuous set-ups using a bimetallic Ni-Cu catalyst with a high metal content. *Catal. Sci. Technol.* **2016**, *6*, 5899–5915. [CrossRef]
32. Asedegbega-Nieto, E.; Guerrero-Ruíz, A.; Rodríguez-Ramos, I. Study of CO chemisorption on graphite-supported Ru–Cu and Ni–Cu bimetallic catalysts. *Thermochim. Acta* **2005**, *434*, 113–118. [CrossRef]
33. Crisafulli, C.; Galvagno, S.; Maggiore, R.; Scirè, S.; Saeli, A. Performance of supported Ru-Cu bimetallic catalysts prepared from nitrate precursors. *Catal. Lett.* **1990**, *6*, 77–83. [CrossRef]

34. Alekseeva, M.V.; Otyuskaya, D.S.; Rekhtina, M.A.; Bulavchenko, O.A.; Stonkus, O.A.; Kaichev, V.V.; Zavarukhin, S.G.; Thybaut, J.W.; Alexiadis, V.; Venderbosch, R.H.; et al. NiCuMo-SiO_2 catalyst for pyrolysis oil upgrading: Model acidic treatment study. *Appl. Catal. A* **2019**, *573*, 1–12. [CrossRef]
35. Mile, B.; Stirling, D.; Zammitt, M.A.; Lovell, A.; Webb, M. The Location of Nickel Oxide and Nickel in Silica-Supported Catalysts: Two Forms of "NiO" and the Assignment of Temperature-Programmed Reduction Profiles. *J. Catal.* **1988**, *114*, 217–229. [CrossRef]
36. Tsay, M.-T.; Chang, F.-W. Characterization of rice husk ash-supported nickel catalysts prepared by ion exchange. *Appl. Catal. A* **2000**, *203*, 15–22. [CrossRef]
37. Ashok, J.; Reddy, P.S.; Raju, G.; Subrahmanyam, M.; Venugopal, A. Catalytic Decomposition of Methane to Hydrogen and Carbon Nanofibers over Ni-Cu-SiO_2 Catalysts. *Energy Fuels* **2009**, *23*, 5–13. [CrossRef]
38. Chen, L.-C.; Lin, S.D. The ethanol steam reforming over Cu-Ni/SiO_2 catalysts: Effect of Cu/Ni ratio. *Appl. Catal. B* **2011**, *106*, 639–649. [CrossRef]
39. Bykova, M.V.; Ermakov, D.Y.; Khromova, S.A.; Smirnov, A.A.; Lebedev, M.Y.; Yakovlev, V.A. Stabilized Ni-based catalysts for bio-oil hydrotreatment: Reactivity studies using guaiacol. *Catal. Today* **2014**, *220–222*, 21–31. [CrossRef]
40. Srivastava, S.; Jadeja, G.C.; Parikh, J. Synergism studies on alumina-supported copper-nickel catalysts towards furfural and 5-hydroxymethylfurfural hydrogenation. *J. Mol. Catal. A: Chem.* **2017**, *426*, 244–256. [CrossRef]
41. Naghash, A.R.; Etsell, T.H.; Xu, S. XRD and XPS Study of Cu-Ni Interactions on Reduced Copper-Nickel-Aluminum Oxide Solid Solution Catalysts. *Chem. Mater.* **2006**, *18*, 2480–2488. [CrossRef]
42. Fedorov, A.V.; Kukushkin, R.G.; Yeletsky, P.M.; Bulavchenko, O.A.; Chesalov, Y.A.; Yakovlev, V.A. Temperature-programmed reduction of model CuO, NiO and mixed CuO–NiO catalysts with hydrogen. *J. Alloys Compd.* **2020**, *844*, 156135. [CrossRef]
43. Wu, Q.; Duchstein, L.D.L.; Chiarello, G.L.; Christensen, J.M.; Damsgaard, C.D.; Elkjær, C.F.; Wagner, J.B.; Temel, B.; Grunwaldt, J.-D.; Jensen, A.D. In Situ Observation of Cu–Ni Alloy Nanoparticle Formation by X-ray Diffraction, X-ray Absorption Spectroscopy, and Transmission Electron Microscopy: Influence of Cu/Ni Ratio. *ChemCatChem* **2014**, *6*, 301–310. [CrossRef]
44. Ermakova, M.A.; Ermakov, D.Y. High-loaded nickel–silica catalysts for hydrogenation, prepared by sol–gel Route: Structure and catalytic behavior. *Appl. Catal. A* **2003**, *245*, 277–288. [CrossRef]
45. Rietveld, H. A profile refinement method for nuclear and magnetic structures. *J. Appl. Crystallogr.* **1969**, *2*, 65–71. [CrossRef]